Structural mechanism of the magnetic phase transitions in $FeTiO_3$

A. Zafar,[1] A. M. Milinda Abeykoon,[2] and V. Petkov[1,*]
[1]*Department of Physics, Central Michigan University, Mt. Pleasant, Michigan 48858, USA*
[2]*Photon Sciences Division, Brookhaven National Laboratory, Upton, New York 11973, USA*

(Received 24 April 2024; accepted 26 August 2024; published 6 September 2024)

The structural mechanism of the magnetic phase transitions in $FeTiO_3$ ilmenite, including the paramagnetic (PM) to antiferromagnetic (AFM) transition induced by reducing temperature in zero magnetic field and the AFM to ferromagnetic (FM) transition induced by applying strong magnetic field at a fixed temperature below the Néel temperature, T_N, are studied by total synchrotron x-ray scattering. It is found that in both cases the concerted effect of Coulomb repulsion, spin-orbit coupling, and exchange interactions is what determines the response of the crystal lattice to variations in external perturbations such as temperature and magnetic field. In particular, due to strong spin-orbit coupling and Coulomb repulsion, Fe and Ti atoms move in sync along the *c* axis of the crystal lattice such that their separation changes by less than 1%. At the same time, due to strong intralayer ferromagnetic interactions, the Fe-O-Fe bond angle becomes closer to 90°. Notably, the direction of the motion occuring during the temperature-induced PM to AFM transition is opposite to that occuring during the magnetic field-induced AFM to FM transition. Altogether, the seemingly simple $FeTiO_3$ ilmenite behaves like a complex physical system where charge, spin, orbital, and lattice degrees of freedom are strongly coupled. Our findings are likely to be relevant to other members of the ilmenite family and spin-orbit coupled magnetic insulators in general.

DOI: 10.1103/PhysRevMaterials.8.093602

I. INTRODUCTION

Recently, transition metal $MTiO_3$ oxides from the ilmenite family, where M = Mn, Fe, Co, or Ni, have gained renewed research interest because of their fascinating physical properties and potential for practical applications in the fields of photocatalysis, spintronics, and optoelectronics [1–6]. In these materials, the partially occupied *d* shells of the metallic species allow for a range of charge and spin states leading to rich phase diagrams of electronic and magnetic phase transitions. Furthermore, the strong spin-orbit coupling together with the competing exchange interactions between the M atoms lead to a strong structural response to external stimuli such as temperature, pressure, and magnetic field [7,8]. For example, $FeTiO_3$ is found to exhibit large spontaneous magnetostriction [9] while $NiTiO_3$ and $CoTiO_3$ exhibit a strong magnetodielectric effect. The temperature of the magnetic ordering in the latter has been found to change with external pressure [9,10]. Mixed ilmenites like (Mn, Fe, Ni)TiO_3 have shown spin glasslike and multiferroic behavior [10,11]. The peculiar properties of the ilmenites are thought to be rooted in their specific layered structure and presence of two distinct types of transition metal atoms.

In particular, oxygen atoms in $FeTiO_3$ form hexagonally packed planes where the metal atoms occupy two-thirds of the octahedral sites between the planes such that octahedra centered by Ti and Fe atoms form layers alternating along the *c* direction of a crystal lattice with an average trigonal space group R-3 symmetry. Each octahedron shares three edges with octahedra from the same layer, a face with an octahedron in an adjacent layer, and a face with a vacant octahedral site [12,13]. Thus, Fe and Ti alternate along the *c* axis of the crystal lattice in a Ti-Fe-vacancy-Fe-Ti sequence, as shown in Fig. 1(a). The near-neighbor metal-metal, e.g., Fe^{2+}-Fe^{2+}, interactions within a layer occur through an octahedral edge, whereas the near-neighbor metal-metal, i.e., Fe^{2+}-Ti^{4+}, interactions along the *c* direction occur through an octahedral face. Because of the relatively short Fe^{2+}-Ti^{4+} separation, which, as reported, is approximately 2.942 Å at room temperature, Fe^{2+} and Ti^{4+} ions from adjacent layers experience a considerable Coulomb repulsion. As a result, both appear displaced from the center of the respective octahedra and form puckered atomic planes, where the metal atoms from each layer experience alternating out-of-plane displacement from their would-be positions in an ideally flat plane running through the center of the respective oxygen octahedra [Fig. 1(b)]. As a result, the bonds between metal atoms and oxygens from a shared octahedral face appear longer than those between metal atoms and oxygens facing an octahedral vacancy [Fig. 1(b)].

At room temperature, the band gap in $FeTiO_3$ amounts to 2.6–2.9 eV. The valence band is formed from O 2*p* and Fe 3*d* orbitals, whereas the conduction band is formed from O 2*p*, Ti 3*d*, and Fe 3*d* orbitals [14,15]. The experimental magnetic moment for Fe^{2+} at 2 K is 4.38 μ_B along the *c* axis and 0.56 μ_B in the *ab* plane of the crystal lattice. Thus, the total magnetic moment amounts to 4.42 μ_B, which is slightly larger than the theoretical value of 4.2 μ_B for octahedrally coordinated Fe^{2+} ions [16–18], indicating that the orbital angular momentum of Fe^{2+} in $FeTiO_3$ is not completely quenched. According to

*Contact author: petko1vg@cmich.edu

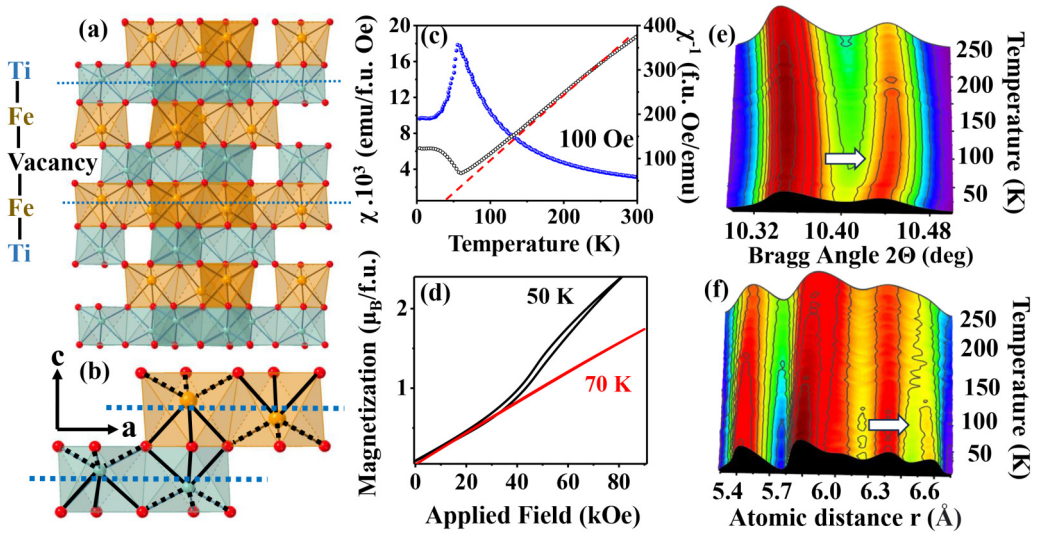

FIG. 1. (a) Stacking of layers of [TiO6] (light blue) and [FeO6] (light brown) octahedra in $FeTiO_3$ along the c axis of the crystal lattice. Cation vacancies in the layers are also shown (white). (b) Close view of [TiO6] and [FeO6] octahedra, highlighting the correlated displacement of Fe and Ti atoms from the centra of the respective octahedra, leading to the presence of short (broken lines) and long (solid lines) metal cation-oxygen bonds. The horizonal blue lines highlight the puckered nature of the planes populated with metal atoms, where adjacent metal atoms are displaced from the center of the oxygen octahedra in an out-of-phase manner. (c) Thermal evolution of the susceptibility (blue) for $FeTiO_3$. It shows a sharp peak at $T_N = 58$ K, where the material becomes an antiferromagnet upon cooling. The inverse susceptibility is also shown. Upon cooling the material, its temperature dependence deviates from linearity below 150 K, indicating the onset of fluctuations of Fe magnetic moments. This dependence is linear above 150 K, which is typical for a paramagnetic material. (d) Field evolution of the magnetization for temperatures above (red) and below (black) T_N. The data obtained at 50 K, i.e., below T_N, show a hysteresis, indicating the emergence of a field-induced ferromagnetic state. The critical field above which the magnetization deviates from linearity is about 40 kOe. Intensity color maps for (e) XRD patterns and (f) atomic PDFs for $FeTiO_3$. Arrows indicate the presence of nonlinearities in the temperature evolution of XRD and PDF data appearing below 150 K. In the color maps, the intensity increases as the color changes from dark blue to dark red.

Goodenough and Stickler [19–21], there are two major types of superexchange interactions between the magnetic moments of Fe^{2+} ions in $FeTiO_3$. One of them is a strong intralayer Fe^{2+}-O-Fe^{2+} interaction with a magnitude of 2.45 meV that is ferromagnetic (FM) in character. The other is a less strong interlayer Fe^{2+}-O-Ti-O-Fe^{2+} interaction with a magnitude of −0.574 meV that is antiferromagnetic in character [22]. Accordingly, $FeTiO_3$ becomes an antiferromagnet (AF) when cooled down to Néel temperature, T_N, as low as 58 K, where the magnetic moments of Fe atoms in each Fe layer are oriented along the c axis of the crystal lattice and parallel to each other, i.e., FM coupled, whereas the magnetic moments of Fe atoms from adjacent layers appear antiparallel, i.e., AF coupled [10,18]. Upon an application of magnetic field below T_N, $FeTiO_3$ has been reported to undergo a metamagnetic phase transition into a FM state where the spins of all Fe atoms appear parallel to each other while preserving their orientation along the c axis of the crystal lattice [22,23]. This is because the magnetocrystalline anisotropy in $FeTiO_3$, which can be expressed in terms of an effective anisotropy field, H_A, of 150 kOe, is very strong. The metamagnetic AFM to FM transition is first order below 35 K and exhibits a critical field, H_c, of 80 kOe at 4.2 K. It is second order in the temperature from 35 K to 58 K, where the critical field is less than 50 kOe and the spins of Fe atoms from adjacent layers do not appear perfectly parallel to each other. Because the crystal symmetry does not change, both the temperature-induced PM to AFM and field-induced AFM to FM transitions appear isostructural. However, significant changes in the lattice parameters have been observed to take place in the vicinity of T_N [9], implying the presence of concurrent changes in the interatomic distances. No clear picture of the way the crystal lattice responds to the onset of magnetic order, be it induced by reducing temperature or applying magnetic field, emerged from the studies conducted so far. Using synchrotron x-ray data and structure modeling, we find that the onset of magnetic order involves a coupled re-arrangement of Fe^{2+} and Ti^{4+} ions inside the oxygen polyhedra, reflecting the concerted effect of Coulomb repulsion, spin-orbit coupling, and exchange interactions in $FeTiO_3$.

II. EXPERIMENT

A. Sample preparation

A $FeTiO_3$ sample was synthesized by a conventional solid-state reaction method. In particular, stoichiometric amounts of Fe_2O_3 ($\geqslant$ 99.99%, Sigma-Aldrich) and TiO_2 ($\geqslant$ 99.99%, Sigma-Aldrich) were mixed thoroughly and ground to fine powder for 2 hr. Then the material was calcined twice at 1100 °C to improve its homogeneity. During the calcination, the heating and cooling rates were kept constant at 10 °C/ min. The calcined sample was again ground for 2 more hours and then pressed into a pellet. To achieve phase purity, the pellet was sintered at 1300 °C for 15 hr, using constant heating and cooling rates of 5 °C/ min. In-house x-ray diffraction (XRD) measurements on fine powder obtained by

crushing the pellet showed that the sample is a single $FeTiO_3$ phase.

B. Magnetic properties characterization

The magnetic properties of $FeTiO_3$ were characterized on a physical property measuring system Dynacool from Quantum Design using the vibrating sample mode of operation. The powder sample was tightly packed in a cylindrical plastic holder with a diameter of 2 mm and the magnetic field applied in a direction perpendicular to its vertical axis. Experimental data for the magnetic susceptibility as a function of temperature are shown in Fig. 1(c). The data were taken upon cooling the sample in a constant magnetic field of 100 Oe. The susceptibility is seen to increase with decreasing temperature and peaks at $T_N = 58$ K, signaling the emergence of AF order. The inverse susceptibility is also shown in Fig. 1(c). In line with results reported in Ref. [9], it is seen to deviate from linearity below 150 K, indicating the onset of fluctuations of the Fe magnetic moments. Experimental data for the magnetization as a function of magnetic field are shown in Fig. 1(d). Data taken at 70 K, i.e., above T_N, scale with the applied field, reflecting the absence of magnetic order. Data taken at 50 K, i.e., below T_N, show a hysteresis, which is characteristic to FM order. The critical field, H_c, for the emergence of FM order appears to be close to 40 kOe, as estimated by the inflection point on the hysteresis curve. In line with prior studies (see Fig. 4 in Ref. [24]), the curve does not show saturation because, at 50 K, the Fe^{2+} spins do not appear completely aligned with the applied magnetic field.

C. Synchrotron x-ray scattering experiments

Synchrotron XRD experiments were performed at the beamline 28-ID-1 at the National Synchrotron Source-II, Brookhaven National Laboratory, using x-rays with energy of 74.46 keV ($\lambda = 0.1665$ Å). The powder sample was tightly packed (packing fraction of about 60%) in a cylindrical Kapton tube with a diameter of 0.8 mm and kept inside a liquid He cryostat used to control its temperature. To improve the powder averaging and counting statistics, the size of the x-ray beam spot on the sample was set to 0.5 mm by 0.5 mm. Scattered x-ray intensities were collected with a PerkinElmer area detector while decreasing the temperature from 300 K to 10 K in steps of 5 K. Two data sets were obtained at each temperature point. One of the data sets was obtained with the detector positioned 1000 mm away from the sample to achieve high resolution in reciprocal space necessary for Rietveld analysis of the crystal structure. The other data set was collected with the detector positioned 204 mm away from the sample to reach high wave vectors, q, ($q_{max} = 28$ Å^{-1} in the current experiment) necessary to obtain high-resolution atomic pair distribution functions (PDFs). The latter were derived from the diffraction patterns using standard procedures [24]. Atomic PDFs have proven to have an extra sensitivity to variations in the local atomic structure of materials [25,26]. Intensity color maps of the experimental high-q_{max} XRD patterns and PDFs derived from them are shown in Figs. 1(e) and 1(f), respectively. Particular Bragg and PDF peaks appear to change their position nonlinearly with temperature below 150 K. The concurrent nonlinearities in the temperature dependence of the magnetic susceptibility and PDF peaks, i.e., interatomic distances, indicate the presence of strong spin-lattice coupling well before the AFM order sets in at T_N.

Synchrotron XRD data were also taken at a fixed temperature of 50 K while applying a magnetic field of strength of up 50 kOe in a direction perpendicular to the Kapton tube, which is the maximum field currently available at synchrotron beamlines suitable for total x-ray scattering studies. Note that a magnetic field of 50 kOe would not trigger an AFM to FM metamagnetic transition at temperatures below 50 K because it is weaker than the critical fields for the transition at these temperatures (see Fig. 5 in Ref. [22]). Representative patterns, taken in steps of 5 kOe, are shown in Fig. S1 ([27]). As can be seen in the figure, no additional Bragg peaks appear but the intensities of existing Bragg peaks change significantly with the strength of the magnetic field. The observation indicates that while the trigonal structure of $FeTiO_3$ is preserved in the field induced FM phase, the material develops a significant crystallographic texture. The texture arises from the high magnetocrystalline anisotropy in $FeTiO_3$, rendering the individual crystallites orient such that their c axis, i.e., Fe spins, align with the direction of the external magnetic field. Significant texture effects have also been reported in neutron diffraction patterns for magnetic field-treated $FeTiO_3$ [9].

III. DIFFRACTION DATA ANALYSIS

A. Crystal structure as a function of temperature

High-q resolution XRD data were subjected to Rietveld analysis using the GSAS-II software package [28]. The analyses were based on the well-known trigonal structure of $FeTiO_3$. The model performed very well at temperatures both above and below T_N, as illustrated in Figs. 2(a) and 2(b). Lattice parameters and unit cell volume derived from the fits are shown in Figs. 3(a) and 3(b). The a lattice parameter is seen to decrease near linearly with decreasing temperature down to 10 K. The c parameter, however, shows a marked nonlinearity with decreasing temperature. As a result, the unit cell volume for $FeTiO_3$ also shows a markedly nonlinear evolution with temperature. Distances between the planes of O atoms sandwiching the puckered planes of Fe, $(O\text{-}O)_{Fe}$, and Ti, $(O\text{-}O)_{Ti}$, atoms are shown in Fig. 3(c) as a function of temperature. The interplane $(O\text{-}O)_{Fe}$ and $(O\text{-}O)_{Ti}$ distances are different, reflecting the different size of Ti (size of $Ti^{4+} = 0.605$ Å) and Fe (size of $Fe^{2+} = 0.78$ Å) ions occupying the octahedral sites between the respective planes. The temperature evolution of the distances is highly nonlinear and resembles that of the c lattice parameter. Distances between metal and oxygen atoms forming the octahedra, i.e., Ti/Fe-O bond lengths, and distances between first neighbor metal atoms from adjacent layers, i.e., interlayer $(Ti\text{-}Ti)_c$, $(Ti\text{-}Fe)_c$, and $(Fe\text{-}Fe)_c$ distances, are shown in Figs. 3(d)–3(f). The distances are seen to change with temperature in a nontrivial manner.

To ascertain the results of the Rietveld analysis, atomic PDFs derived from the high-q_{max} XRD data were also fit with the space group R-3 structure model using the software PDFgui [29]. The model performed very well both at temperatures above and temperatures below T_N, as illustrated

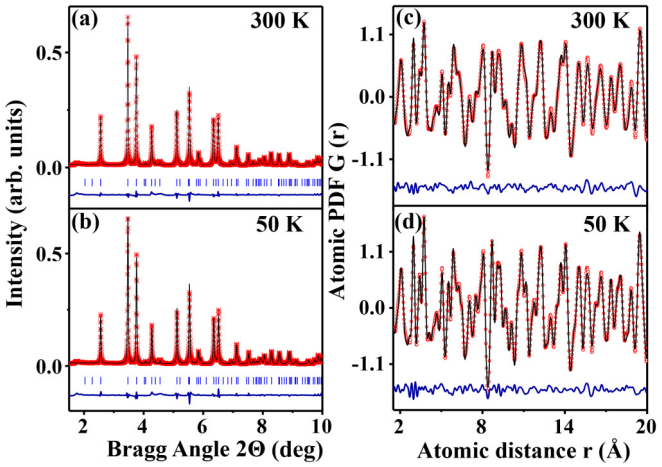

FIG. 2. Rietveld fits (red line) to high-q resolution XRD patterns (symbols) for $FeTiO_3$ collected at (a) 300 K and (b) 50 K. Vertical blue lines show the position of Bragg peaks. The residual difference (blue color) is shifted for the sake of clarity. The fit agreement factor, R_{WP}, is about 8% for both fits. Fits (black line) to atomic PDFs (red symbols) obtained at (c) 300 K and (d) 50 K. Here the residual difference (blue color) is also shifted for the sake of clarity. The fit agreement factor, R_{WP}, is about 11% for both fits. All fits are based on a space group R-3 type structure model [12]. Representative crystal structure data resulted from Rietveld and PDF fits are given in Table S1.

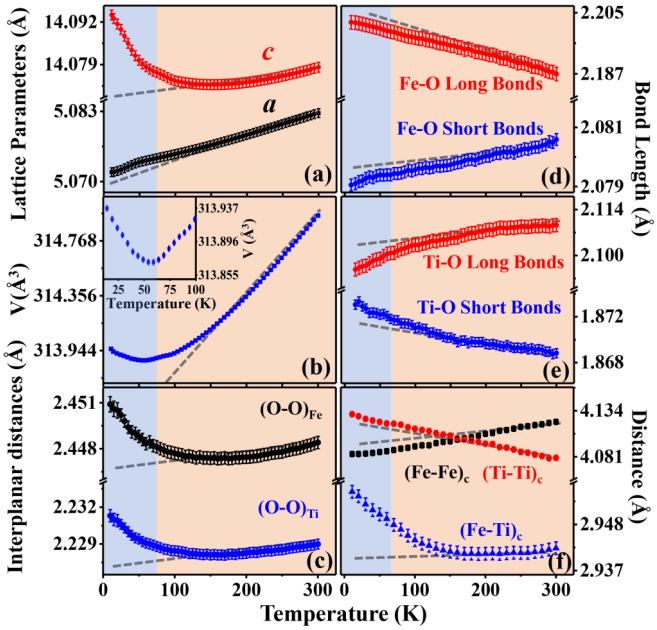

FIG. 3. Temperature evolution of the (a) a and c lattice parameters, (b) unit cell volume, V, (c) distance between oxygen planes, $(O\text{-}O)_{Ti}$ and $(O\text{-}O)_{Fe}$, sandwiching Ti-centered and Fe-centered octahedra, respectively, (d) long and short Fe-O bonding distances, (e) long and short Ti-O bonding distances, and (f) metal-metal distances along the c axis of the crystal lattice. Data are derived from Rietveld fits to experimental XRD data. Light blue and brown shaded areas highlight temperature regions where the material is an antiferromagnet and paramagnet, respectively. Gray broken lines emphasize nonlinearities in the presented data appearing below 100 K. All data sets show a nonlinear behavior with temperature. The nonlinearity is particularly well expressed with the c lattice parameter. The size of the symbols in (b) and (f) is commensurate with the respective error bars.

in Figs. 2(c) and 2(d). Lattice parameters, unit cell volume, and interplanar and Fe/Ti-O bonding distances computed from the refined models are summarized in Fig. S2 [27]. The PDF- and Rietveld-fit-derived values for the respective structure parameters summarized in Figs. 3 and S2 differ by less than 1%, i.e., are very similar. Their temperature evolution is also similar, indicating that both locally and on average $FeTiO_3$ responds to external perturbations, in particular temperature variation, in a largely similar manner. The most noticeable difference is that between the temperature evolutions of the PDF-refined and Rietveld-refined c lattice parameter, which start deviating from linearity at about 150 K and 100 K, respectively [data in Fig. 3(a) vs data in Fig. S2a]. The observation indicates that, locally, the spin-lattice coupling in $FeTiO_3$ is stronger in comparison to the average crystal structure. This may explain why, locally, the temperature evolution of coupled Fe^{2+}-Ti^{4+}, Ti^{4+}-Ti^{4+}, and Fe^{2+}-Fe^{2+} separations appear somewhat different in comparison to the average crystal structure [compare data in Fig. 3(f) vs data in Fig. S2f].

B. Crystal structure as a function of magnetic field

An intensity color map for the (006) Bragg peak is shown in Fig. 4(a). The intensity change is due to the formation of a [00l]-type crystallographic texture, arising from the strong magnetocrystalline anisotropy (effective H_A of 150 kOe) in $FeTiO_3$. The latter renders the crystallites reorient such that the c axis of the crystal lattice lines up with the direction of the applied magnetic field. The intensity changes start in a field close to 20 kOe and are near complete at a field of 40 kOe, which is close to the critical field for inducing FM order at 50 K [see Fig. 1(c) and Fig. 5 in Ref. [22]). The XRD data

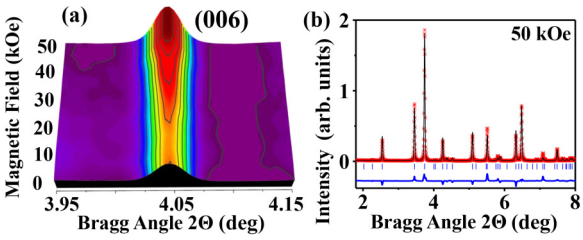

FIG. 4. (a) Color map of the intensity of (006) Bragg peak in the XRD patterns for $FeTiO_3$ obtained at 50 K while the magnetic field has been varied between zero and 50 kOe. Changes in the intensity start at 20 kOe, which is below the critical field H_c of 40 kOe for the AFM to FM transition and level off at H_c of about 40 kOe. The data show that, due to the large magneto-crystalline anisotropy, $FeTiO_3$ crystallites rotate in magnetic field such that the spins of Fe atoms, i.e., the trigonal c axis, align with the direction of the field. (b) Rietveld fit to a XRD pattern obtained at 50 K in magnetic field of 50 kOe. The fit is based on a space group R-3-type structure model [14] exhibiting a strong [001] crystallographic texture. Vertical blue bars show positions of Bragg peaks. The residual difference (blue line) is shifted for clarity. The fit agreement factor, R_{WP}, is about 12%. In the color map in (a) the intensity increases as the color changes from magenta to dark red.

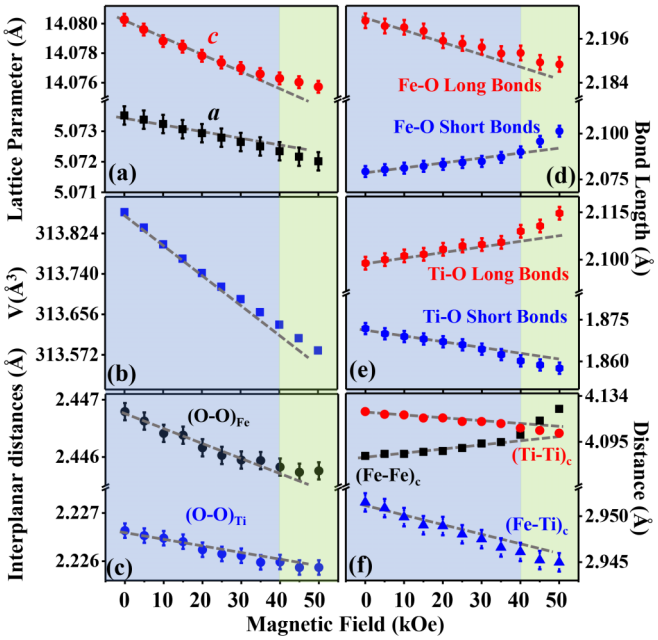

FIG. 5. Magnetic field evolution of the (a) *a* and *c* lattice parameters, (b) unit cell volume, *V*, (c) distance between oxygen planes, $(O\text{-}O)_{Ti}$ and $(O\text{-}O)_{Fe}$, sandwiching Ti-centered and Fe-centered octahedra, respectively, (d) long and short Fe-O bonding distances, (e) long and short Ti-O bonding distances, and (f) metal-metal distances along the *c* axis of the crystal lattice. Data are derived from Rietveld fits to experimental XRD data. Light blue and green shaded areas highlight magnetic field regions where the material exhibits antiferromagnetic and ferromagnetic order, respectively. The critical field, H_c, between the two magnetic orders is at about 40 kOe. Gray broken lines emphasize nonlinearities in the presented data appearing in the vicinity of H_c. The size of the symbols in (b) and (f) is commensurate with the respective error bars.

obtained in fields weaker than 20 kOe were successfully fit with a model based on a trigonal space group R-3-type symmetry. The XRD data obtained in fields stronger than 20 kOe were successfully fit with the same structure model using the March-Dollase correction [30] for a [00l] preferred crystallographic orientation (texture) implemented in the GSAS-II software package. Attempts to fit the data without a texture correction or using other crystallographic directions of preferred orientation were unsuccessful, as demonstrated in Fig. S3. From the March-Dollase parameter, the degree of [00l] preferred orientation at 50 kOe was estimated to be close to 47%, indicating that a very large fraction of the crystallites in the studied sample have responded strongly to the applied magnetic field and are likely to have undergone a second order AFM to FM transition. The latter is not a surprise because the experimental data for magnetization [Fig. 1(d)] clearly show that such a transition takes place in $FeTiO_3$ powders. Lattice parameters, unit cell volume, interplanar and Fe/Ti-O bonding distances computed from the refined models [31] are summarized in Fig. 5. Computational procedures for PDF analysis on polycrystalline materials exhibiting crystallographic texture are, however, not well developed [32,33]. Therefore, we did not consider the magnetic field obtained XRD data in real space in terms of the respective atomic PDFs.

IV. DISCUSSION

Upon decreasing temperature, usually, materials tend to shrink because atomic vibration amplitudes diminish, leading to an increase in the atomic packing density and/or decrease in bond lengths. This behavior is exhibited by $FeTiO_3$ when it is cooled down from room temperature to about 100 K [see Fig. 3(a)]. The shrinking reduces the unit cell volume by about 0.3% [Fig. 3(b)], where the major contributor to the volume decrease is the decrease in the *a* lattice parameter. Below this temperature, the *a* parameter keeps decreasing, but the material shows an unusual thermal expansion leading to a slight increase in the atomic volume. This is because, after the initial decrease, the separation between the densely packed oxygen planes, $(O\text{-}O)_{Fe}$ and $(O\text{-}O)_{Ti}$, starts increasing leading to an increase in the *c* lattice parameter below 100 K, which offsets the concurrent gradual decrease in the *a* parameter [see Figs. 3(a)–3(c)]. Overall, the unit cell volume of $FeTiO_3$ shrinks by about 0.25% when it is cooled down from room temperature to 10 K. Interestingly, the motion of the Fe^{2+} and Ti^{4+} ions positioned between the oxygen layers appears decoupled from that of the layers. In particular, upon decreasing temperature, Ti^{4+} ions tend to move towards the center of the respective polyhedra, leading to an increase and decrease in the short and long Ti^{4+}-O distances, respectively. Likely because of the strong Coulombic repulsion, Fe^{2+} ions move in sync with Ti^{4+} ions such that the Fe^{+2}-Ti^{+4} average separation increases from 2.942(1) Å at room temperature to 2.956(1) Å at 10 K, i.e., by 0.5% [Figs. 6(a) and 6(b)]. Concurrently, the Fe^{2+}-Fe^{2+} separation decreases from 4.121(1) Å to 4.084(1) Å, i.e., by about 0.9%. As a result, the Fe^{2+} off-centering increases, leading to a further decrease and increase in the short and long Fe^{2+}-O distances, respectively. In the process, the puckering of the planes of Ti^{4+} ions decreases [puckering amplitude of 0.633(1) Å at 300 K vs puckering amplitude of 0.594(1) Å at 50 K]. On the other hand, that of the planes of Fe^{2+} ions increases [puckering amplitude of 0.583(1) Å at 300 K vs puckering amplitude of 0.648(1) Å at 50 K; see Figs. 6(a) and 6(b)].

As can be seen in Fig. 5(a), similarly to pressure [34–36], isothermally applied magnetic field reduces both lattice parameters of $FeTiO_3$ Fig. 5(a), leading to a further 0.2% reduction of the unit cell volume in comparison to the value attained by reducing the temperature to 50 K Fig. 5(b). Accordingly, the oxygen layers become more densely packed with magnetic field, as demonstrated by the further decreased values of $(O\text{-}O)_{Fe}$ and $(O\text{-}O)_{Ti}$ distances Fig. 5(c). Furthermore, the magnetic field pushes the Fe^{2+} ions towards the center of respective octahedra, leading to an increase and decrease in the short and long Fe^{2+}-O distances, respectively Fig. 5(d). Contrary to the case of reducing temperature, however, it tends to increase the off-centering of the magnetically inactive Ti^{4+} ions a bit, leading to a small decrease and increase of the short and long Ti^{4+}-O distances, respectively Fig. 5(e). Overall, the Fe^{2+}-Ti^{4+} separation diminishes in comparison to the 50 K value by 0.2% (2.944(1) Å at 50 K in field of 50 kOe vs 2.951(1) Å at 50 K in zero magnetic field), indicative of an enhanced interaction between the Fe^{2+} and Ti^{4+} ions, which counteracts the Coulomb repulsion between them. The enhancement could include a partial charge transfer be-

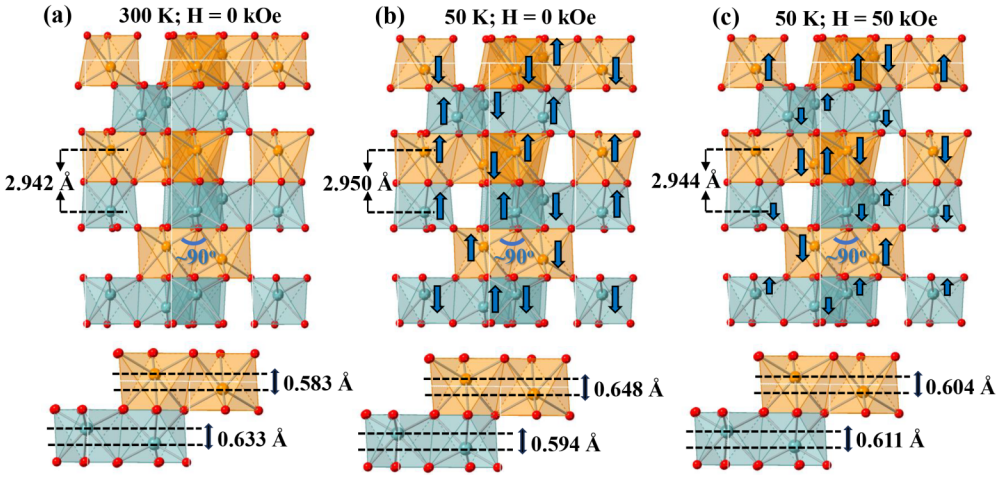

FIG. 6. (a) Stacking of [TiO6] (light blue) and [FeO6] (light brown) octahedra in $FeTiO_3$ along the c axis of the crystal lattice, with the shortest distance between Fe and Ti atoms along the c axis shown, as derived from fits to experimental XRD data obtained at 300 K in zero magnetic field. The correlated displacement of Ti and Fe atoms from the centra of the respective octahedra (pair of horizontal broken lines and the respective amplitude of puckering) is also shown. (b) Same as in (a), as derived from fit to experimental XRD data obtained at 50 K in zero magnetic field. (c) same as in (a), as derived from fit to experimental XRD data obtained at 50 K in magnetic field of 50 kOe. Vertical blue arrows in (b) and (c) indicate the direction of the displacement of metal ions upon decreasing temperature in zero magnetic field and increasing magnetic field at constant temperature, respectively. The length of the arrows reflects the magnitude of the displacements. The puckering of Ti and Fe planes changes significantly with changing temperature or magnetic field. At any temperature and magnetic field intensity, the Fe-O-Fe bond angle appears close to 90°, consistent with FM superexchange interactions in the Fe layers. The models in (a) and (b) are based on structure data derived from the Rietveld fits shown in Figs. 2(a) and 2(b), respectively. The model in (c) is based on structure data derived from the Rietveld fit in Fig. 4(b).

tween their $3d_z^2$ orbitals, possibly leading to a partial magnetic polarization of Ti^{4+} ions, as discussed in Refs. [15,37–39]. As a result, the Fe^{2+}-Fe^{2+} distance increases by 0.9% to a value of 4.123(1) Å. This is close to the Fe^{2+}-Fe^{2+} distance in room temperature $FeTiO_3$, where, however, the unit cell volume is 0.5% larger. In the process, the puckering of the planes of Ti^{4+} ions increases (puckering amplitude of 0.594(1) Å at 50 K in zero field vs puckering amplitude of 0.611(1) Å at 50 K in field of 50 kOe). On the other hand, that of the planes of Fe^{2+} ions decreases (puckering amplitude of 0.648(1) Å at 50 K in zero field vs puckering amplitude of 0.604(1) Å at 50 K in field of 50 kOe; see Figs. 6(b) and 6(c)). Notably, the observed changes in the lattice parameters, interlayer and Ti/Fe bonding distances start as soon as magnetic field is applied and seem to accelerate when the field approaches 40 kOe, which is the critical field for triggering a second order AFM to FM transition in $FeTiO_3$ at 50 K.

It is known that the type and strength of superexchange interactions in $FeTiO_3$ depend on structural parameters such as distances between Fe^{2+} ions, Fe^{2+}-O bond lengths and Fe^{2+}-O- Fe^{2+} bond angles, i.e., on the relative position of Fe^{2+} and oxygen ions with respect to each other. Upon cooling, Fe^{2+} ions from adjacent octahedra in PM $FeTiO_3$ start moving along the c direction of the crystal lattice, but the motion is such that the intralayer bond Fe^{2+}-O- Fe^{2+} angles increase from 89.09(1)° to 89.37(1)° (see Fig. S4), which is consistent with a strengthening of the intralayer FM interactions between the spins of Fe^{2+} ions. The motion, however, brings the Fe^{2+} ions facing a common octahedral vacancy closer together, as measured by the observed 1% decrease in the interplanar Fe^{2+}-Fe^{2+} distance in comparison to the 10 K value. This would increase the direct overlap between their $3d_z^2$ orbitals, thus promoting interlayer AFM interactions [40–44]. This may explain the emergence of cooperative AF order in $FeTiO_3$ at low temperatures, where the spins of Fe atoms in the layers remain ferromagnetically coupled while those of Fe atoms from adjacent layers arrange antiparallel to each other [see Figs. 1(d) and 5].

Upon the application of magnetic field, Fe^{2+} ions in AFM $FeTiO_3$ also start moving along the c axis of the crystal lattice such that the intralayer Fe^{2+}-O- Fe^{2+} bond angle increases from 89.26(1)° to 89.44(1)° (see Fig. S3), consistent with a further strengthening of the intralayer FM interactions. The motion, however, increases the distance between the Fe^{2+} ions facing a common octahedral vacancy by 0.9%, which would decrease the direct overlap between their $3d_z^2$ orbitals and destabilize the interlayer AFM interactions. In the process, the unit cell volume decreases, eventually leading to changes in the overlap between O $2p$ and Fe $3d$ orbitals along the c axis of the crystal lattice and, hence, how the superexchange interaction between the spins of Fe^{2+} ions from adjacent layers propagates through Ti-O layers between them (see Fig. 4 in Ref. [42]). This may explain the emergence of interlayer FM coupling, leading to a second-order AFM to FM phase transition [see Fig. 1(d)] when the applied field surpasses 40 kOe. It is tempting to assume that the same scenario applies to the first-order AFM to FM transition, which takes place at lower temperatures. Future in situ studies of the type conducted here are necessary to verify this assumption, which will require improved synchrotron beamline instrumentation, including magnets delivering steady state fields well in excess of 50 kOe.

V. CONCLUSIONS

In $FeTiO_3$, the orbital angular momentum of Fe^{2+} ions is not quenched, and, due to strong spin-orbit coupling, Fe^{2+} spins appear tightly bound to the c axis of the trigonal crystal lattice [45]. In addition, the spins of Fe atoms from the puckered Fe layers experience strong superexchange interactions with FM character, which keeps them parallel to each other. Therefore, as our data show, upon reducing temperature and/or application of magnetic field, Fe atoms appear constrained to move along the c axis of the crystal lattice while the "ferromagnetic" Fe^{2+}-O-Fe^{2+} bond angle becomes closer to 90°. Due to the strong Coulomb repulsion between Fe^{2+} and Ti^{4+} ions, however, the latter also appear constrained to move along the c direction of the crystal lattice, where the motion is such that the separation between Fe^{2+} and Ti^{4+} increases slightly. Notably, upon reducing temperature, the motion results in a decrease in the interlayer Fe^{2+}-Fe^{2+} distances, promoting an PM to AFM phase transition. This trend is reversed when magnetic field is applied, leading to a decrease and increase in the Fe^{2+}-Ti^{4+} and Fe^{2+}-Fe^{2} distances, respectively, which facilitates the emergence of FM order. Altogether, it appears that the concerted effect of Coulomb repulsion, spin-orbit coupling, and exchange interactions is what determines the specific mechanism via which the crystal lattice in $FeTiO_3$ responds to external perturbations. In this respect, the seemingly simple $FeTiO_3$ ilmenite appears to behave as other strongly correlated systems [46], where, though coupled, temperature and magnetic field are not necessarily equivalent control parameters to induce phase transitions.

ACKNOWLEDGMENTS

This work was supported by the U.S. Department of Energy, Office of Science, Office of Basic Energy Sciences under Award No. DE-SC0021973. It also used resources of the National Synchrotron Light Source at the Brookhaven National Laboratory provided by the DOE Office of Science under Contract No. DE-SC0012704. Thanks are due to E. Razia for useful discussions.

[1] T. Fujii, M. Kayano, Y. Takada, M. Nakanishi, and J. Takada, Ilmenite–hematite solid solution films for novel electronic devices, Solid State Ion. **172**, 289 (2004).

[2] Z. Dai, P. Zhu, S. Yamamoto, A. Miyashita, K. Narum, and H. Naramoto, Pulsed laser deposition of ilmenite $FeTiO_3$ epitaxial thin film onto sapphire substrate, Thin Solid Films **339**, 114 (1999).

[3] F. Zhou, S. Kotru, and R. K. Pandey, Nonlinear current–voltage characteristics of ilmenite–hematite ceramic, Mater. Lett. **57**, 2104 (2003).

[4] T. Dietl and H. Ohno, Ferromagnetic III–V and II–VI semiconductors, MRS Bull. **28**, 714 (2003).

[5] X. Tang and K. Hu, The formation of ilmenite $FeTiO_3$ powders by a novel liquid mix and H_2/H_2O reduction process, J. Mater. Sci. **41**, 8025 (2006).

[6] F. Ye and A. Ohmori, The photocatalytic activity and photoabsorption of plasma sprayed $TiO_2-Fe_3O_4$ binary oxide coatings, Surf. Coat. Technol. **160**, 62 (2002).

[7] K. Dey, S. Sauerland, J. Werner, Y. Skourski, M. Abdel-Hafiez, R. Bag, S. Singh, and R. Klingeler, Magnetic phase diagram and magnetoelastic coupling of $NiTiO_3$, Phys. Rev. B **101**, 195122 (2020).

[8] M. Hoffmann, K. Dey, J. Werner, R. Bag, J. Kaiser, H. Wadepohl, Y. Skourski, M. Abdel-Hafiez, S. Singh, and R. Klingeler, Magnetic phase diagram, magnetoelastic coupling, and Grüneisen scaling in $CoTiO_3$, Phys. Rev. B **104**, 014429 (2021).

[9] M. Charilaou, D. Sheptyakov, J. F. Löffler, and A. U. Gehring, Large spontaneous magnetostriction in $FeTiO_3$ and adjustable magnetic configuration in Fe (III)-doped $FeTiO_3$, Phys. Rev. B **86**, 024439 (2012).

[10] J. K. Harada, L. Balhorn, J. Hazi, M. C. Kemei, and R. Seshadri, Magnetodielectric coupling in the ilmenites $MTiO_3$ (M = Co, Ni), Phys. Rev. B **93**, 104404 (2016).

[11] H. Kawano, H. Yoshizawa, A. Ito, and K. Motoya, Two successive spin glass transitions in nondiluted Heisenberg-like spin glass $Ni_{0.42}Mn_{0.58}TiO_3$, J. Phys. Soc. Jpn. **62**, 2575 (1993).

[12] G. Shirane, S. J. Pickart, R. Nathans, and Y. Ishikawa, Neutron-diffraction study of antiferromagnetic $FeTiO_3$ and its solid solutions with α-Fe_2O_3, J. Phys. Chem. Solids **10**, 35 (1959).

[13] N. C. Wilson, J. Muscat, D. Mkhonto, P. E. Ngoepe, and N. M. Harrison, Structure and properties of ilmenite from first principles, Phys. Rev. B **71**, 075202 (2005).

[14] G. Radtke, S. Lazar, and G. A. Botton, High-resolution EELS investigation of the electronic structure of ilmenites, Phys. Rev. B **74**, 155117 (2006).

[15] S. W. Chen, M. J. Huang, P. A. Lin, H. T. Jeng, J. M. Lee, S. C. Haw, S. A. Chen, H. J. Lin, K. T. Lu, D. P. Chen *et al.*, Orbital structure of $FeTiO_3$ ilmenite investigated with polarization-dependent x-ray absorption spectroscopy and band structure calculations, Appl. Phys. Lett. **102**, 042107 (2013).

[16] J. J. Stickler, S. Kern, A. Wold, and G. S. Heller, Magnetic resonance and susceptibility of several ilmenite powders, Phys. Rev. **164**, 765 (1967).

[17] R. H. Aguilera-del-Toro, M. Arruabarrena, A. Leonardo, and A. Ayuela, Magnetic order and magnetic anisotropy in two-dimensional ilmenenes, Nanoscale Adv. **5**, 2813 (2023).

[18] H. Kato, Y. Yamaguchi, M. Yamada, S. Funahashi, Y. Nakagawa, and H. Takei, Neutron scattering study of magnetic excitations in oblique easy-axis antiferromagnet $FeTiO_3$, J. Phys. C: Solid State Phys. **19**, 6993 (1986).

[19] J. B. Goodenough and J. J. Stickler, Theory of the magnetic properties of the ilmenites $MTiO_3$, Phys. Rev. **164**, 768 (1967).

[20] J. Kanamori, Magnetic properties of the iron-group anhydrous chlorides, Prog. Theor. Phys. **20**, 890 (1958).

[21] J. B. Goodenough, Direct cation-cation interactions in several oxides, Phys. Rev. **117**, 1442 (1960).

[22] H. Kato, M. Yamada, H. Yamauchi, H. Hiroyoshi, H. Takei, and H. Watanabe, Metamagnetic phase transitions in $FeTiO_3$, J. Phys. Soc. Jpn. **51**, 1769 (1982).

[23] H. Kato and Y. Nakagawa, Dynamics of first-order magnetic phase transition: Relaxation phenomena of metamagnetism in $FeTiO_3$, Phys. B: Condens. Matter **201**, 80 (1994).

[24] P. Juhás, T. Davis, C. L. Farrow, and S. J. L. Billinge, PDFgetX3: A rapid and highly automatable program for processing powder diffraction data into total scattering pair distribution functions, J. Appl. Cryst. **46**, 560 (2013).

[25] V. Petkov, in *Pair Distribution Functions Analysis, Characterization of Materials*, edited by E. N. Kaufmann (Wiley, New York, 2012).

[26] T. Egami and S. J. L. Billinge, *Underneath the Bragg Peaks Structural Analysis of Complex Materials* (Pergamon Press, Amsterdam, 2003).

[27] See Supplemental Material at http://link.aps.org/supplemental/10.1103/PhysRevMaterials.8.093602 for results from atomic PDF analysis.

[28] B. H. Toby and R. B. Von Dreele, GSAS-II: The genesis of a modern open-source all purpose crystallography software package, J. Appl. Cryst. **46**, 544 (2013).

[29] C. L. Farrow, P. Juhas, J. W. Liu, D. Bryndin, E. S. Božin, J. Bloch, Th. Proffen, and S. J. L. Billinge, PDFfit2 and PDFgui: Computer programs for studying nanostructure in crystals, J. Phys.: Condens. Matter **19**, 335219 (2007).

[30] E. Zolotoyabko, Determination of the degree of preferred orientation within the March-Dollase approach, J. Appl. Cryst. **42**, 513 (2009).

[31] Note that powder samples exhibiting 100% texture are unsuitable for Rietveld analysis because many of the Bragg peaks appear completely attenuated.

[32] Z. Gong and S. J. L. Billinge, Atomic pair distribution functions (PDFs) from textured polycrystalline samples fundamentals, arXiv:1805.10342.

[33] S. Y. Harouna-Mayer, S. Tao, Z. Gong, M. V. Zimmermann, D. Koziej, A. C. Dippel, and S. J. L. Billinge, Real-space texture and pole-figure analysis using the 3D pair distribution function on a platinum thin film, IUCrJ **9**, 594 (2022).

[34] B. A. Wechsler and C. T. Prewitt, Crystal structure of ilmenite ($FeTiO_3$) at high temperature and at high pressure, Amer. Miner. **69**, 176 (1984).

[35] L. C. Ming, Y. H. Kim, T. Uchida, Y. Wang, and M. Rivers, In situ x-ray diffraction study of phase transitions of $FeTiO_3$ at high pressures and temperatures using a large-volume press and synchrotron radiation, Amer. Miner. **91**, 120 (2006).

[36] X. Wu, G. Steinle-Neumann, O. Narygina, I. Kantor, C. McCammon, S. Pascarelli, G. Aquilanti, V. Prakapenka, and L. Dubrovinsky, Iron oxidation state of $FeTiO_3$ under high pressure, Phys. Rev. B **79**, 094106 (2009).

[37] T. Yamanaka, Structural changes induced by lattice–electron interactions: SiO_2 stishovite and $FeTiO_3$ ilmenite, J. Synchrotron Radiat. **12**, 566 (2005).

[38] M. O. J. Y. Hunault, W. Khan, J. Minár, T. Kroll, D. Sokaras, P. Zimmermann, M. U. Delgado-Jaime, and F. M. F. de Groot, Local vs nonlocal states in $FeTiO_3$ probed with 1s2pRIXS: Implications for photochemistry, Inorg. Chem. **56**, 10882 (2017).

[39] T. Fujii, M. Yamashita, S. Fujimori, Y. Saitoh, T. Nakamura, K. Kobayashi, and J. Takada, Large magnetic polarization of Ti^{4+} ions in $FeTiO_3$, J. Magn. Magn. Mater. **310**, e555 (2007).

[40] R. A. Ribeiro, A. M. de Andrade, L. H. S. Lacerda, C. Alexandre Jr, and S. R. de Lázaro, Interplay between interatomic distance and orbital overlap at control of magnetism in $FeBO_3$ (B = Ti, Ge, Zr, Sn) ilmenites, Rev. Process. Químicos **9**, 195 (2015).

[41] R. A. P. Ribeiro, A. Camilo Jr., and S. R. de Lazaro, Electronic structure and magnetism of new ilmenite compounds for spintronic devices: $FeBO_3$ (B = Ti, Hf, Zr, Si, Ge, Sn), J. Magn. Magn. Mater. **394**, 463 (2015).

[42] R. A. P. Ribeiro and S. R. de Lázaro, Structural, electronic and elastic properties of $FeBO_3$ (B = Ti, Sn, Si, Zr) ilmenite: A density functional theory study, RSC Adv. **4**, 59839 (2014).

[43] X. Zhang, B. Lu, R. Li, C. Fan, Z. Liang, and P. Han, Structural, electronic and optical properties of ilmenite $ATiO_3$ (A = Fe, Co, Ni), Mater. Sci. Semicond. Process. **39**, 6 (2015).

[44] X. -C. Zhang, C. M. Fan, Z. H. Liang, and P. D. Han, Electronic structures and optical properties of ilmenite-type hexagonal $ZnTiO_3$, Acta Phys.-Chim. Sin. **27**, 47 (2011).

[45] P. F. McDonald, A. Parasiris, R. K. Pandey, B. L. Gries, and W. P. Kirk, Paramagnetic resonance and susceptibility of ilmenite $FeTiO_3$ crystal, J. Appl. Phys. **69**, 1104 (1991).

[46] V. Petkov, T. D. Rao, A. M. Abeykoon, J. R. Galeano-Cabral, and K. Wei, Spin-lattice coupling in magnetocaloric $Gd_5(Ge, Si)_4$ alloys by in-situ x-ray pair distribution analysis in magnetic field, Phys. Rev. Mater. **6**, 104407 (2022).